

Parametric Down-Conversion and Polariton Pair Generation in Optomechanical Systems

Yong-Chun Liu, Yun-Feng Xiao,* You-Ling Chen, Xiao-Chong Yu, and Qihuang Gong[†]

*Department of Physics and State Key Laboratory for Mesoscopic Physics, Peking University,
Beijing 100871, People's Republic of China*

(Received 6 May 2013; published 20 August 2013; publisher error corrected 17 September 2013)

We demonstrate that the nonlinear optomechanical interaction leads to parametric down-conversion, capable of generating polariton pairs formed by photons and phonons. The nonlinearity is resonantly enhanced through frequency matching, and such parametric down-conversion does not require the stringent condition that the single-photon optomechanical coupling strength g be on the order of the mechanical resonance frequency ω_m . We provide analytical results for the frequency matching condition and derive the nonlinear coefficient. Numerical simulations on polariton pair generation are presented, showing that photonlike polaritons, phononlike polaritons, and mixed photon-phonon polaritons can be selectively generated. Such nonlinear interaction offers a promising way for harnessing the optomechanical nonlinearity to manipulate photons and phonons.

DOI: [10.1103/PhysRevLett.111.083601](https://doi.org/10.1103/PhysRevLett.111.083601)

PACS numbers: 42.50.Wk, 07.10.Cm, 42.65.-k

Optomechanical systems offer the prospect of exploring the quantum properties of mechanical resonators [1–4]. Recent theoretical and experimental efforts have demonstrated parametric oscillation [5,6], optomechanical cooling close to the ground state [7–20], optomechanically induced transparency [21–24], optical wavelength conversion [25,26], normal mode splitting [27,28], and quantum-coherent coupling between optical modes and mechanical modes [29,30]. These progresses mainly rely on the light-enhanced linear optomechanical interaction, which does not possess the ability of generating nonclassical quantum states. Theoretical studies show that the optomechanical nonlinearity can be exploited in the regime of single-photon strong coupling [31–34] with weak laser input. However, in such a regime, the nonlinear interaction is essentially off resonant, and prominent nonlinearity requires that the oscillator displacement exerted by a single photon is comparable with its zero-point uncertainty; namely, the single-photon optomechanical coupling strength g should be on the order of the mechanical resonance frequency ω_m .

Here, we analyze the optomechanical nonlinearity beyond the weakly driven single-photon strong coupling regime and show that under the background of linear optomechanical coupling, the nonlinear interaction can be strongly enhanced through the frequency matching condition. The light-enhanced linear optomechanical coupling leads to the splitting of normal modes and the formation of photon-phonon polaritons, and then frequency matching results in the resonant nonlinear interaction between these polaritons. We analytically derive the frequency matching condition and the enhanced nonlinear coefficient. It is demonstrated that photonlike polaritons, phononlike polaritons, and mixed photon-phonon polaritons can be generated selectively by tuning the laser input.

We consider a generic optomechanical system where a laser-driven optical cavity mode a couples to a mechanical

mode b [Fig. 1(a)]. In the rotating frame at the driving laser frequency ω_L , the system Hamiltonian is given by [35] $H = -(\omega_L - \omega_c)a^\dagger a + \omega_m b^\dagger b + ga^\dagger a(b + b^\dagger) + (\Omega a^\dagger + \Omega^* a)$, where ω_c (ω_m) is the resonance frequency of the optical (mechanical) mode, g denotes the single-photon optomechanical coupling rate, and Ω represents the laser driving strength. Under the displacement transformation $a \equiv a_1 + \alpha$, $b \equiv b_1 + \beta$, with α and β being classical mean values, the driving term can be eliminated, and the Hamiltonian is rewritten as $H = H_L + H_{NL}$, where $H_L = -\Delta a_1^\dagger a_1 + \omega_m b_1^\dagger b_1 + (Ga_1^\dagger + G^* a_1)(b_1 + b_1^\dagger)$ and $H_{NL} = ga_1^\dagger a_1(b_1^\dagger + b_1)$. Here, $G \equiv g\alpha$ describes the light-enhanced optomechanical coupling strength, and $\Delta \equiv \omega_L - \omega_c + 2|G|^2/\omega_m$ is the detuning where optomechanical coupling has been taken into account; H_L represents the quadratic Hamiltonian which leads to linear dynamics, and H_{NL} denotes the nonlinear term. Without loss of generality, in the following, we assume G to be real and positive.

The linear Hamiltonian H_L describes coupled harmonic oscillators, which can be transformed to the normal mode

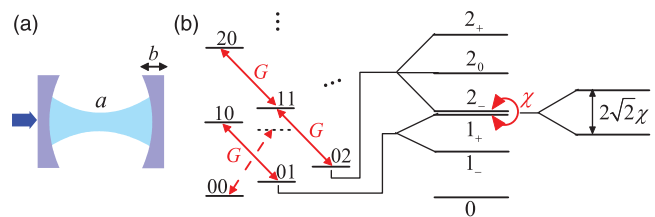


FIG. 1 (color). (a) Sketch of an optically driven optomechanical system. (b) Energy level diagram of the system. $|nm\rangle$ represents a state of n photons and m phonons. $|0\rangle$ denotes the ground state, $|1_{\pm}\rangle$ represent the one-excitation subspace, and $|2_{\pm}\rangle$ and $|2_0\rangle$ represent the two-excitation subspace. χ denotes the nonlinear coefficient.

representation $H_L = \omega_+ c_+^\dagger c_+ + \omega_- c_-^\dagger c_-$. Here, ω_\pm are the eigenfrequencies satisfying $2\omega_\pm^2 = \Delta^2 + \omega_m^2 \pm [(\Delta^2 - \omega_m^2)^2 - 16G^2\Delta\omega_m]^{1/2}$, and c_\pm are the eigenmodes (polariton modes) with the transformation $(a_1 \ b_1)^T = \mathbf{U}(c_+ \ c_- \ c_+^\dagger \ c_-^\dagger)^T$, where \mathbf{U} is a 2×4 matrix described by

$$\mathbf{U} = \begin{pmatrix} \mu_1 & \mu_2 & \mu_3 & \mu_4 \\ \nu_1 & \nu_2 & \nu_3 & \nu_4 \end{pmatrix}. \quad (1)$$

For the red-detuned resonant case $\Delta = -\omega_m$, we obtain $\mu_{1,3} = \nu_{1,3} = (\sqrt{\omega_m/\omega_+} \pm \sqrt{\omega_+/\omega_m})/(2\sqrt{2})$, $\nu_{2,4} = -\mu_{2,4} = (\sqrt{\omega_m/\omega_-} \pm \sqrt{\omega_-/\omega_m})/(2\sqrt{2})$ with $\omega_\pm = \sqrt{\omega_m^2 \pm 2G\omega_m}$, corresponding to the equal-weight mode mixing. In Fig. 1(b), we plot the energy levels for this resonant case with the total excitation numbers being 0, 1, and 2. It shows that the linear coupling G results in two independent sets of sublevels, which correspond to the two normal modes c_+ and c_- .

In previous studies, H_{NL} is only considered when the optical driving is weak ($G \ll g$). However, this is reasonable only in the frequency mismatching regime. As we show now, under strong optical driving, this nonlinear interaction can be resonantly enhanced when the frequency matching condition $\omega_+ = 2\omega_-$ is satisfied. As shown in Fig. 1(b), 1_+ represents the first excited state of mode c_+ , and 2_- denotes the second excited state of mode c_- . With frequency matching, these two states are degenerate, while H_{NL} leads to nonlinear interaction between them. In this case, the resonant interaction conserves the energy and therefore has prominent advantages over the off-resonant interaction in the weak driving case, which suffers from the reduction of nonlinearity by a factor of g/ω_m .

Figure 2(a) plots the frequency mismatch $(\omega_+ - 2\omega_-)/\omega_m$ as a function of detuning Δ and linear coupling strength G . It shows that frequency matching $\omega_+ = 2\omega_-$ can be achieved for the Δ ranging from $-2\omega_m$ to $-\omega_m/2$, with the corresponding optimized coupling strength G_{opt} in the stable region. The reason for $-2\omega_m < \Delta < -\omega_m/2$ is that the linear coupling G tends to push the energy levels to the opposite direction, namely, $\omega_+ > \max(|\Delta|, \omega_m)$ and $\omega_- < \min(|\Delta|, \omega_m)$, and thus the frequency matching requires $\max(|\Delta|, \omega_m)/\min(|\Delta|, \omega_m) < 2$. More explicitly, it is obtained from the normal mode eigenfrequencies that $G_{opt} = [(\Delta^2 - 4\omega_m^2)(4\Delta^2 - \omega_m^2)/(\Delta\omega_m)]^{1/2}/10$, corresponding to the red curve in Fig. 2(a). The sensitivity of the optimal coupling strength G_{opt} to the detuning Δ is plotted in Fig. 2(b), which shows that the frequency matching condition is robust to the variation of laser detuning in a wide range except for the regions near $\Delta = -2\omega_m$ and $\Delta = -\omega_m/2$. Under the frequency matching condition, the eigenfrequencies of the two polariton modes read $\omega_+ = 2\omega_- = 2\sqrt{(\Delta^2 + \omega_m^2)}/5$, which are plotted in Fig. 2(c). It shows that $\omega_+ \simeq -\Delta$ and $\omega_- \simeq \omega_m$ near

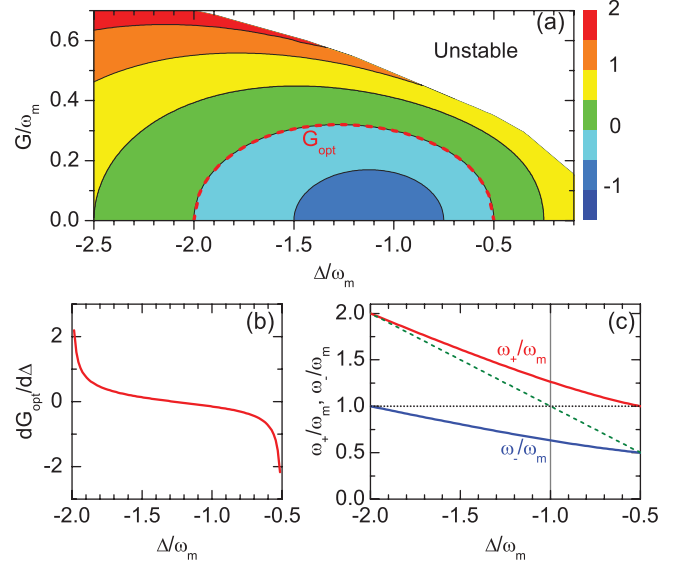


FIG. 2 (color). (a) Contour plot of $(\omega_+ - 2\omega_-)/\omega_m$ as a function of Δ and G . The dashed red curve denotes $\omega_+ = 2\omega_-$. The white region in the top right corner indicates the unstable region. (b) $dG_{opt}/d\Delta$ as a function of Δ . (c) ω_+/ω_m (solid red curve) and ω_-/ω_m (solid blue curve) as functions of Δ for $G = G_{opt}$ [along the dashed red curve in (a)]. The dashed green line denotes $-\Delta/\omega_m$, and the dotted black line denotes 1. The gray vertical line denotes $\Delta/\omega_m = -1$.

$\Delta = -2\omega_m$ while $\omega_+ \simeq \omega_m$ and $\omega_- \simeq -\Delta$ near $\Delta = -\omega_m/2$, revealing the detuning-dependent role reversal of the polariton modes.

As a perturbation, H_{NL} can be reexpressed in the normal mode basis described by $H_{NL} = f(c_+, c_-, c_+^\dagger, c_-^\dagger)$. Under the condition $g \ll \omega_m$, we apply the rotating-wave approximation and neglect high-frequency off-resonant terms. The resultant Hamiltonian is

$$H_{NL} \simeq -\chi(c_+^\dagger c_-^2 + c_+ c_-^\dagger{}^2), \quad (2)$$

which corresponds to the parametric down-conversion Hamiltonian; i.e., the annihilation of a c_+ mode polariton leads to the generation of a pair of c_- mode polaritons. The parameter χ corresponds to the nonlinear coefficient, given by

$$\chi = [(\mu_1\mu_2 + \mu_3\mu_4)(\nu_2 + \nu_4) + \mu_2\mu_4(\nu_1 + \nu_3)]g. \quad (3)$$

In Fig. 3(a), the nonlinear parameter χ as a function of Δ is plotted, showing that χ is on the order of g for broad detunings, which is of great advantage over the weak driving case where the nonlinear parameter scales as g^2/ω_m . Note that the major contribution in Eq. (3) is the term $\mu_1\mu_2\nu_2g$, corresponding to the optomechanical interaction of the form $a_1^\dagger a_1(b_1^\dagger + b_1)$, which involves three photon (phonon) annihilation and creation processes: one photon acts as a c_+ polariton, the other photon acts as a c_- polariton, and the phonon acts as a c_- polariton.

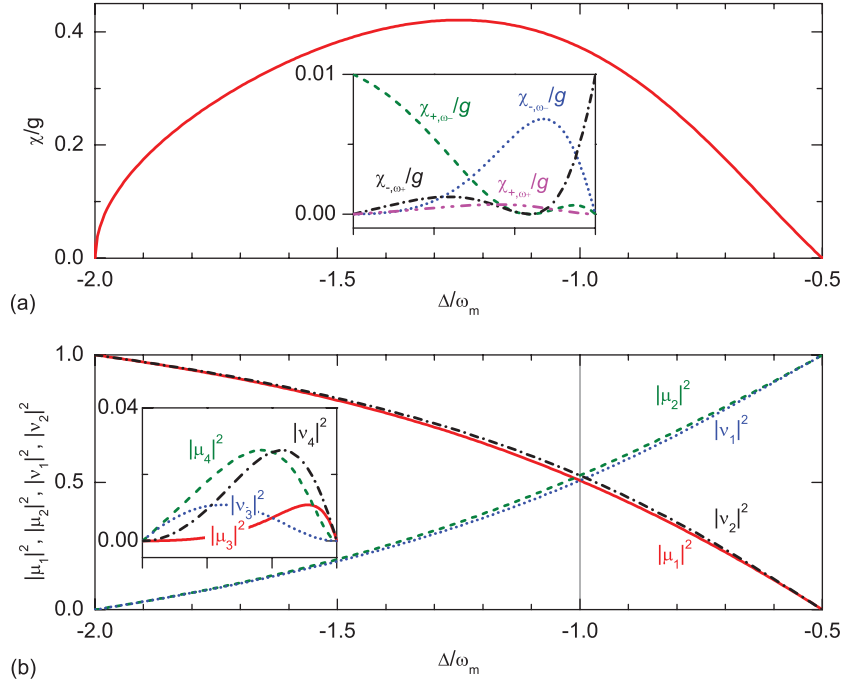


FIG. 3 (color). (a) χ/g as a function of Δ , given by Eq. (3). Inset: $\chi_{+, \omega_-}/g$ (dashed green curve), $\chi_{-, \omega_-}/g$ (dotted blue curve), $\chi_{-, \omega_+}/g$ (dash-dotted black curve), and $\chi_{+, \omega_+}/g$ (two-dot-dashed magenta curve) as functions of Δ for $g/\omega_m = 0.01$. (b) $|\mu_1|^2$ (solid red curve), $|\mu_2|^2$ (dashed green curve), $|\nu_1|^2$ (dotted blue curve), and $|\nu_2|^2$ (dash-dotted black curve) as functions of Δ . The gray vertical line denotes $\Delta/\omega_m = -1$. Inset: $|\mu_3|^2$ (solid red curve), $|\mu_4|^2$ (dashed green curve), $|\nu_3|^2$ (dotted blue curve) and $|\nu_4|^2$ (dash-dotted black curve) as functions of Δ .

The maximum of χ locates at $\Delta_{\max} \simeq -1.25\omega_m$, with $\chi_{\max} \simeq 0.42g$. The reason why χ_{\max} is not obtained in the linear resonant case ($\Delta = -\omega_m$, $\chi = 0.37g$) is that this interaction is asymmetric between c_+ and c_- polaritons, which involves one c_+ polariton and two c_- polaritons. For the strongest interaction, the c_+ polariton is more photonlike while the c_- polariton is more phononlike. It is noted that the major off-resonant nonlinear interaction terms include $\tilde{\chi}_{+, \omega_-} c_+^\dagger c_+ (c_- + c_-^\dagger)$, $\tilde{\chi}_{-, \omega_-} c_-^\dagger c_- (c_+ + c_+^\dagger)$, $\tilde{\chi}_{-, \omega_+} c_-^\dagger c_- (c_+ + c_+^\dagger)$, and $\tilde{\chi}_{+, \omega_+} c_+^\dagger c_+ (c_- + c_-^\dagger)$. The corresponding effective nonlinear parameters are described by $\chi_{\pm, \omega_-} = \tilde{\chi}_{\pm, \omega_-}^2 / \omega_-$ and $\chi_{\pm, \omega_+} = \tilde{\chi}_{\pm, \omega_+}^2 / \omega_+$, which are plotted in the inset of Fig. 3(a) for comparison with χ . It reveals that these off-resonant nonlinear parameters are strongly reduced due to the far-detuned interaction, typically on the order of $(g/\omega_m)\chi$.

Figure 3(b) plots the coefficients $|\mu_k|^2$ and $|\nu_k|^2$ ($k = 1, 2$) as functions of Δ . Here, $|\mu_1|^2$ and $|\nu_1|^2$ describe the photonic and phononic components of the c_+ polariton, while $|\mu_2|^2$ and $|\nu_2|^2$ describe the photonic and phononic components of the c_- polariton. For $\Delta \simeq -2\omega_m$, the c_+ mode is photonlike while the c_- mode is phononlike, and it is opposite for $\Delta \simeq -\omega_m/2$. As the detuning Δ varies from $-2\omega_m$ to $-\omega_m/2$, the c_- polariton has less phononic components, and $-2\omega_m < \Delta < -\omega_m$ corresponds to the phonon-pair-dominated region, while $-\omega_m < \Delta < -\omega_m/2$ corresponds to the photon-pair-dominated region.

Note that the small discrepancy between $|\mu_1|^2$ and $|\nu_2|^2$ ($|\mu_2|^2$ and $|\nu_1|^2$) originates from the anti-rotating-wave interaction characterized by $|\mu_k|^2$ and $|\nu_k|^2$ ($k = 3, 4$), which are plotted in Fig. 3(b).

We perform numerical simulations to identify such parametric down-conversion interaction. In addition to the coherent evolution described by the Hamiltonian H , the incoherent evolution caused by dissipations is included by considering the master equation

$$\dot{\rho} = i[\rho, H] + \kappa \mathcal{D}[a_1]\rho + \gamma(n_{\text{th}} + 1)\mathcal{D}[b_1]\rho + \gamma n_{\text{th}} \mathcal{D}[b_1^\dagger]\rho, \quad (4)$$

where ρ is the density operator of the system, $\mathcal{D}[\delta]\rho = \delta\rho\delta^\dagger - (\delta^\dagger\delta\rho + \rho\delta^\dagger\delta)/2$ denotes the standard dissipator in Lindblad form, κ and γ represent the decay rates of the optical and mechanical modes, and $n_{\text{th}} = 1/[e^{\hbar\omega_m/(k_B T)} - 1]$ is the thermal phonon number at the environmental temperature T .

In Fig. 4, the simulation results of polariton pair generation are plotted. For the linear resonant case $\Delta = -\omega_m$, corresponding to the equal-weight mixing of photons and phonons, we use a single-photon state as the initial condition to examine the mixed photon-phonon polariton pair generation. As shown in Fig. 4(a), at $t = 0$, the populations of c_\pm polaritons are almost the same, and then c_+ polaritons convert to c_- polariton pairs. At $t \sim 100/\omega_m$, more than

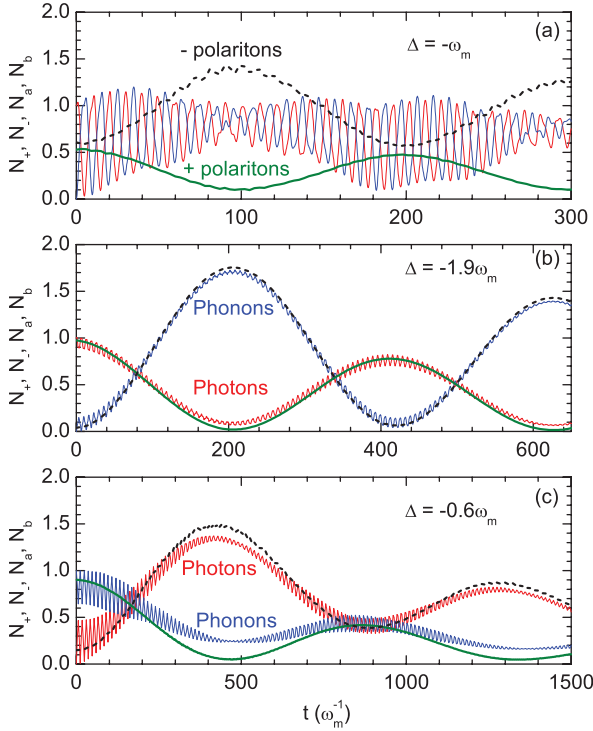


FIG. 4 (color). Time evolution of + polariton number N_+ (thick green curves), - polariton number N_- (dashed black curves), mean photon number N_a (thin red curves), and phonon number N_b (thin blue curves) for $\Delta = -\omega_m$ (a), $-1.9\omega_m$ (b), and $-0.6\omega_m$ (c). Other parameters: $G = G_{\text{opt}}$, $g/\omega_m = 0.03$, $\kappa/\omega_m = 10^{-3}$, $\gamma/\omega_m = 10^{-5}$, and $n_{\text{th}} = 0$.

80% of c_+ polaritons are converted to c_- polaritons. Here, the c_- polariton mode can be expressed as $c_- = -0.73(a_1 - b_1) + 0.16(a_1^\dagger - b_1^\dagger)$, which consists of equal components of optical and mechanical modes. It shows that the photon and phonon numbers are oscillating, with a period of $\sim \pi/G$, which is a result of background linear optomechanical coupling. In Fig. 4(b), we consider $\Delta = -1.9\omega_m$, which is located at the phonon-pair-dominant region. It reveals that the photon (phonon) almost behaves the same as the c_+ (c_-) polariton, since the c_+ (c_-) mode consists of 97% optical (mechanical) component. With a single-photon input, the photonlike polariton has effectively converted to a pair of phononlike polaritons at $t \sim 200/\omega_m$. Compared with Fig. 4(a), the time scale is longer due to the smaller nonlinear coefficient $\chi = 0.17g$. Because of the dissipation, the maximum phonon number is slightly less than 2. In Fig. 4(c), we plot the results for the photon-pair-dominated case $\Delta = -0.6\omega_m$ with a single-phonon initial state. It reveals that photonlike polariton pairs can also be generated at the end of the half-oscillation period $t \simeq 480/\omega_m$.

We further demonstrate that the polariton pair generation is also robust to both the frequency mismatch and the thermal noise. As an example without loss of generality, we investigate the phononlike polariton pair generation processes ($\Delta = -1.9\omega_m$) under the frequency matching and

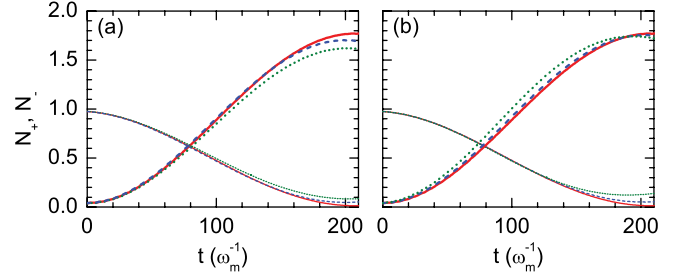


FIG. 5 (color online). Time evolution of + polariton number N_+ (thin curves) and - polariton number N_- (thick curves) for (a) various δ and (b) various n_{th} . In (a), $n_{\text{th}} = 0$; $\delta = 0$ (solid red curve), $0.004\omega_m$ (dashed blue curve), and $-0.004\omega_m$ (dotted green curve). In (b), $G = G_{\text{opt}}$; $n_{\text{th}} = 0$ (solid red curve), 30 (dashed blue curve), and 100 (dotted green curve). In (a) and (b), $\Delta = -1.9\omega_m$ and other parameters are the same as Fig. 4.

mismatch conditions, as shown in Fig. 5(a). Here, we define the frequency mismatch parameter $\delta \equiv \omega_+ - 2\omega_-$ to characterize the off-resonant parametric down-conversion. In the plots, $\delta = \pm 0.004\omega_m$ correspond to laser frequency drift of $\mp 0.005\omega_m$. Therefore, for a mechanical resonance frequency $\omega_m/(2\pi) = 3.68$ GHz [8], the polariton pair generation process is only slightly affected if the frequency drift is within 18 MHz. In real experiments, with mode locking, the frequency drift can reach and even exceed 1 MHz. In addition, for the region $-1.9\omega_m < \Delta < -0.6\omega_m$, due to a more robust frequency matching condition [Fig. 2(b)] than that for $\Delta = -1.9\omega_m$, the polariton pair generation processes can tolerate even larger frequency drifts.

Note that the mechanical mode should be cooled close to the ground state to suppress the thermal noise. Since the laser is red detuned in the range of $-2\omega_m < \Delta < -\omega_m/2$, the driving laser is capable of cooling the mechanical mode near the ground state before the polariton pair generation processes start [20,36]. In Fig. 5(b), we plot the phononlike polariton pair generation dynamics under various thermal phonon numbers n_{th} . For $\omega_m/(2\pi) = 3.68$ GHz, the bath temperature $T \sim 20$ K corresponds to the thermal phonon number $n_{\text{th}} \sim 100$ [8]. In this case, the polariton pair generation processes are robust enough to the thermal heating. For room temperature $T \sim 300$ K, corresponding to $n_{\text{th}} \sim 1500$, ground state cooling is limited by the small cavity decay rate κ in this strong coupling regime and the polariton pair generation processes will be affected. However, using the dynamic dissipative cooling protocol in Ref. [20], it is promising to improve the cooling process and suppress the thermal noise.

In summary, we have examined the optomechanical nonlinearity for $g \ll \omega_m$ and find the resonant enhancement of the nonlinearity under the linear optomechanical coupling background. We show that such enhanced nonlinear interaction has parametric down-conversion form and can be observed for a red-detuned input laser with

detuning Δ in the range of $-2\omega_m < \Delta < -\omega_m/2$. The nonlinear coefficient is on the order of g with its maximal value $\sim 0.42g$ at $\Delta \simeq -1.25\omega_m$. We demonstrate that the nonlinear interaction enables the generation of mixed photon-phonon polaritons. In particular, near $\Delta = -2\omega_m$, phononlike polaritons are efficiently generated, while near $\Delta = -\omega_m/2$, photonlike polaritons can be created. This provides a new tool for exploiting the nonlinear interactions in optomechanical systems.

We thank H.-K. Li for helpful discussions. This work was supported by the 973 Program (Grants No. 2013CB328704 and No. 2013CB921904), NSFC (Grants No. 11004003, No. 11222440, No. 11121091, and No. 91221304), and RFDPH (Grant No. 20120001110068).

Note added.—Recently, we noticed two related works on the arXiv, Refs. [37,38].

*yfxiao@pku.edu.cn;

www.phy.pku.edu.cn/~yfxiao/index.html

†qhgong@pku.edu.cn

- [1] T.J. Kippenberg and K.J. Vahala, *Science* **321**, 1172 (2008).
- [2] F. Marquardt and S.M. Girvin, *Physics* **2**, 40 (2009).
- [3] I. Favero and K. Karrai, *Nat. Photonics* **3**, 201 (2009).
- [4] D. van Thourhout and J. Roels, *Nat. Photonics* **4**, 211 (2010).
- [5] T. Carmon, H. Rokhsari, L. Yang, T.J. Kippenberg, and K.J. Vahala, *Phys. Rev. Lett.* **94**, 223902 (2005).
- [6] T.J. Kippenberg, H. Rokhsari, T. Carmon, A. Scherer, and K.J. Vahala, *Phys. Rev. Lett.* **95**, 033901 (2005).
- [7] J.D. Teufel, T. Donner, D. Li, J.W. Harlow, M.S. Allman, K. Cicak, A.J. Sirois, J.D. Whittaker, K.W. Lehnert, and R.W. Simmonds, *Nature (London)* **475**, 359 (2011).
- [8] J. Chan, T.P.M. Alegre, A.H. Safavi-Naeini, J.T. Hill, A. Krause, S. Gröblacher, M. Aspelmeyer, and O. Painter, *Nature (London)* **478**, 89 (2011).
- [9] S. Gigan, H.R. Böhm, M. Paternostro, F. Blaser, G. Langer, J.B. Hertzberg, K.C. Schwab, D. Bäuerle, M. Aspelmeyer, and A. Zeilinger, *Nature (London)* **444**, 67 (2006).
- [10] O. Arcizet, P.-F. Cohadon, T. Briant, M. Pinard, and A. Heidmann, *Nature (London)* **444**, 71 (2006).
- [11] A. Schliesser, P. Del’Haye, N. Nooshi, K.J. Vahala, and T.J. Kippenberg, *Phys. Rev. Lett.* **97**, 243905 (2006).
- [12] A. Schliesser, R. Rivière, G. Anetsberger, O. Arcizet, and T.J. Kippenberg, *Nat. Phys.* **4**, 415 (2008).
- [13] S. Gröblacher, J.B. Hertzberg, M.R. Vanner, G.D. Cole, S. Gigan, K.C. Schwab, and M. Aspelmeyer, *Nat. Phys.* **5**, 485 (2009).
- [14] Y.-S. Park and H. Wang, *Nat. Phys.* **5**, 489 (2009).
- [15] A. Schliesser, O. Arcizet, R. Rivière, G. Anetsberger, and T.J. Kippenberg, *Nat. Phys.* **5**, 509 (2009).
- [16] T. Rocheleau, T. Ndukum, C. Macklin, J.B. Hertzberg, A.A. Clerk, and K.C. Schwab, *Nature (London)* **463**, 72 (2009).
- [17] I. Wilson-Rae, N. Nooshi, W. Zwerger, and T.J. Kippenberg, *Phys. Rev. Lett.* **99**, 093901 (2007).
- [18] F. Marquardt, J.P. Chen, A.A. Clerk, and S.M. Girvin, *Phys. Rev. Lett.* **99**, 093902 (2007).
- [19] C. Genes, D. Vitali, P. Tombesi, S. Gigan, and M. Aspelmeyer, *Phys. Rev. A* **77**, 033804 (2008).
- [20] Y.-C. Liu, Y.-F. Xiao, X. Luan, and C.W. Wong, *Phys. Rev. Lett.* **110**, 153606 (2013).
- [21] S. Weis, R. Rivière, S. Deléglise, E. Gavartin, O. Arcizet, A. Schliesser, and T.J. Kippenberg, *Science* **330**, 1520 (2010).
- [22] A.H. Safavi-Naeini, T.P.M. Alegre, J. Chan, M. Eichenfield, M. Winger, Q. Lin, J.T. Hill, D.E. Chang, and O. Painter, *Nature (London)* **472**, 69 (2011).
- [23] G.S. Agarwal and S. Huang, *Phys. Rev. A* **81**, 041803(R) (2010).
- [24] K. Qu and G.S. Agarwal, *Phys. Rev. A* **87**, 031802(R) (2013).
- [25] J.T. Hill, A.H. Safavi-Naeini, J. Chan, and O. Painter, *Nat. Commun.* **3**, 1196 (2012).
- [26] C. Dong, V. Fiore, M.C. Kuzyk, and H. Wang, *Science* **338**, 1609 (2012).
- [27] S. Gröblacher, K. Hammerer, M.R. Vanner, and M. Aspelmeyer, *Nature (London)* **460**, 724 (2009).
- [28] J.M. Dobrindt, I. Wilson-Rae, and T.J. Kippenberg, *Phys. Rev. Lett.* **101**, 263602 (2008).
- [29] E. Verhagen, S. Deléglise, S. Weis, A. Schliesser, and T.J. Kippenberg, *Nature (London)* **482**, 63 (2012).
- [30] T.A. Palomaki, J.W. Harlow, J.D. Teufel, R.W. Simmonds, and K.W. Lehnert, *Nature (London)* **495**, 210 (2013).
- [31] P. Rabl, *Phys. Rev. Lett.* **107**, 063601 (2011).
- [32] A. Nunnenkamp, K. Børkje, and S.M. Girvin, *Phys. Rev. Lett.* **107**, 063602 (2011).
- [33] M. Ludwig, A.H. Safavi-Naeini, O. Painter, and F. Marquardt, *Phys. Rev. Lett.* **109**, 063601 (2012).
- [34] K. Stannigel, P. Komar, S.J.M. Habraken, S.D. Bennett, M.D. Lukin, P. Zoller, and P. Rabl, *Phys. Rev. Lett.* **109**, 013603 (2012).
- [35] C.K. Law, *Phys. Rev. A* **51**, 2537 (1995).
- [36] I. Wilson-Rae, N. Nooshi, J. Dobrindt, T.J. Kippenberg, and W. Zwerger, *New J. Phys.* **10**, 095007 (2008).
- [37] M.-A. Lemonde, N. Didier, and A.A. Clerk, *Phys. Rev. Lett.* **111**, 053602 (2013).
- [38] K. Børkje, A. Nunnenkamp, J.D. Teufel, and S.M. Girvin, *Phys. Rev. Lett.* **111**, 053603 (2013).